CHEMISTRY OF MATERIALS

Article

pubs.acs.org/cm

Elucidating the Mechanism of Silica Nanoparticle PEGylation Processes Using Fluorescence Correlation Spectroscopies

Kai Ma, Duhan Zhang, Ying Cong, and Ulrich Wiesner*

Department of Materials Science and Engineering, Cornell University, Ithaca, New York 14850, United States

Supporting Information

ABSTRACT: Surface modification with polyethylene glycol (PEG; PEGylation) is a widely used technique to improve nanoparticle (NP) stability, biocompatibility, and biodistribution profiles. In particular, PEGylation of silica surfaces and coatings plays a pivotal role across various classes of NPs. Despite the use of numerous protocols there is limited fundamental understanding of the mechanisms of these processes for NPs. Here, after reaction optimization for particle stability, we employ fluorescence correlation and cross-correlation spectroscopy (FCS, FCCS) on ultrasmall (<10 nm) fluorescent silica nanoparticles (SNPs) in water as a test bed. We show unexpected fast reaction kinetics in successful PEGylation observed even at nanomolar concentrations and attributed this to instant noncovalent adsorption of PEG molecules to the SNP surface preceding covalent attachment. Further studies of various reaction conditions enable the elucidation of process design criteria for NP PEGylation and surface modification with functional ligands, which may be applicable to a broad range of NPs thereby accelerating progress in fields ranging from biosensing to nanomedicine.

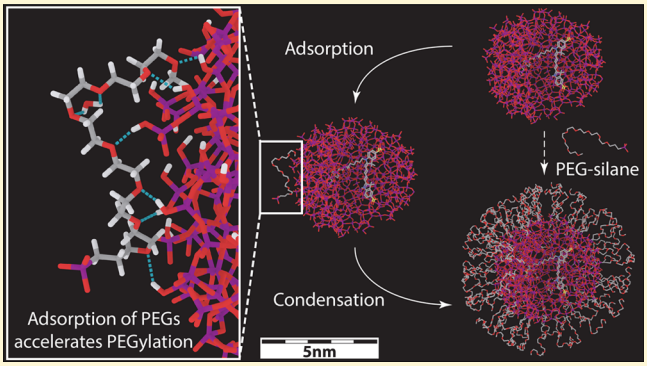

INTRODUCTION

The global market for nanomedicine is expected to grow with an annual rate of 12.3% and reach a value of >170 billion in 2019.[1] As one of the most promising nanomedicine candidates, multifunctional organic−inorganic hybrid NPs have attracted significant research attention worldwide for both imaging/diagnostics and therapeutics.[2−5] However, in order to successfully translate hybrid NPs from the laboratory to the clinic, PEGylation is an essential step to endow NPs with long-term stability as well as favorable biodistribution and pharmacokinetics (PK) profiles.[6−8] In the past decade, silica coating techniques have been established to stabilize inorganic NPs in aqueous media without disturbing their physical properties.[9] Therefore, the PEGylation of silica surfaces and coatings plays a pivotal role for nanomedicine applications across various classes of nanomaterials, including dense[10] and mesoporous silica nanoparticles (SNPs),[11,12] quantum dots,[13] gold NPs,[14,15] magnetic NPs,[16] graphene,[17] and carbon nanotubes.[18]

Compared to the well-studied PEGylation of pharmaceuticals,[19] e.g., proteins and peptides, the PEGylation of NPs enabling desirable biodistribution and PK often remains challenging due to the complexity of the interfacial reactions between NP surfaces and ligand molecules.[20,21] Despite the use of numerous protocols to PEGylate specific NPs,[22] little is known mechanistically about how this process proceeds, which in turn hampers the production of clinically translatable nanomaterials. To that end, here we take advantage of highly tunable silica sol−gel chemistry and use ultrasmall (<10 nm diameter) fluorescent SNPs, referred to as Cornell prime dots (C′ dots),[10] as a test bed to study the PEGylation mechanism of silica surfaces.[23,24] Compared to larger NPs, ultrasmall SNPs are more sensitive to surface reactions due to the enhanced particle surface to volume ratio.[25] Furthermore, using ultrasmall SNPs it is possible to work with relatively short PEG ligands (molar mass <1000 g/mol) for which the effects of different polymer conformations on the particle surface are less significant, thereby reducing the complexity of the kinetics of attachment.[26] Finally, work on ultrasmall SNPs is particularly relevant as such <10 nm diameter particles have recently been successfully translated into the clinic,[27] and multiple human clinical trials are currently ongoing.

Conventional techniques to characterize the result of NP PEGylation reactions include dynamic light scattering (DLS),[28] thermogravimetric analysis (TGA),[29] nuclear magnetic resonance (NMR) spectroscopy,[30] and Raman analysis.[31] These techniques provide detailed information on PEG loading and conformation on particle surfaces; however, little mechanistic insight is gained about how a successful PEGylation process proceeds. Fluorescence correlation spectroscopy, FCS, exploits fluorescence fluctuations caused by diffusion of molecular spices in a confocal setup to analyze their concentrations and

Received: January 4, 2016
Revised: February 6, 2016
Published: February 8, 2016

DOI: 10.1021/acs.chemmater.6b00030
Chem. Mater. 2016, 28, 1537−1545

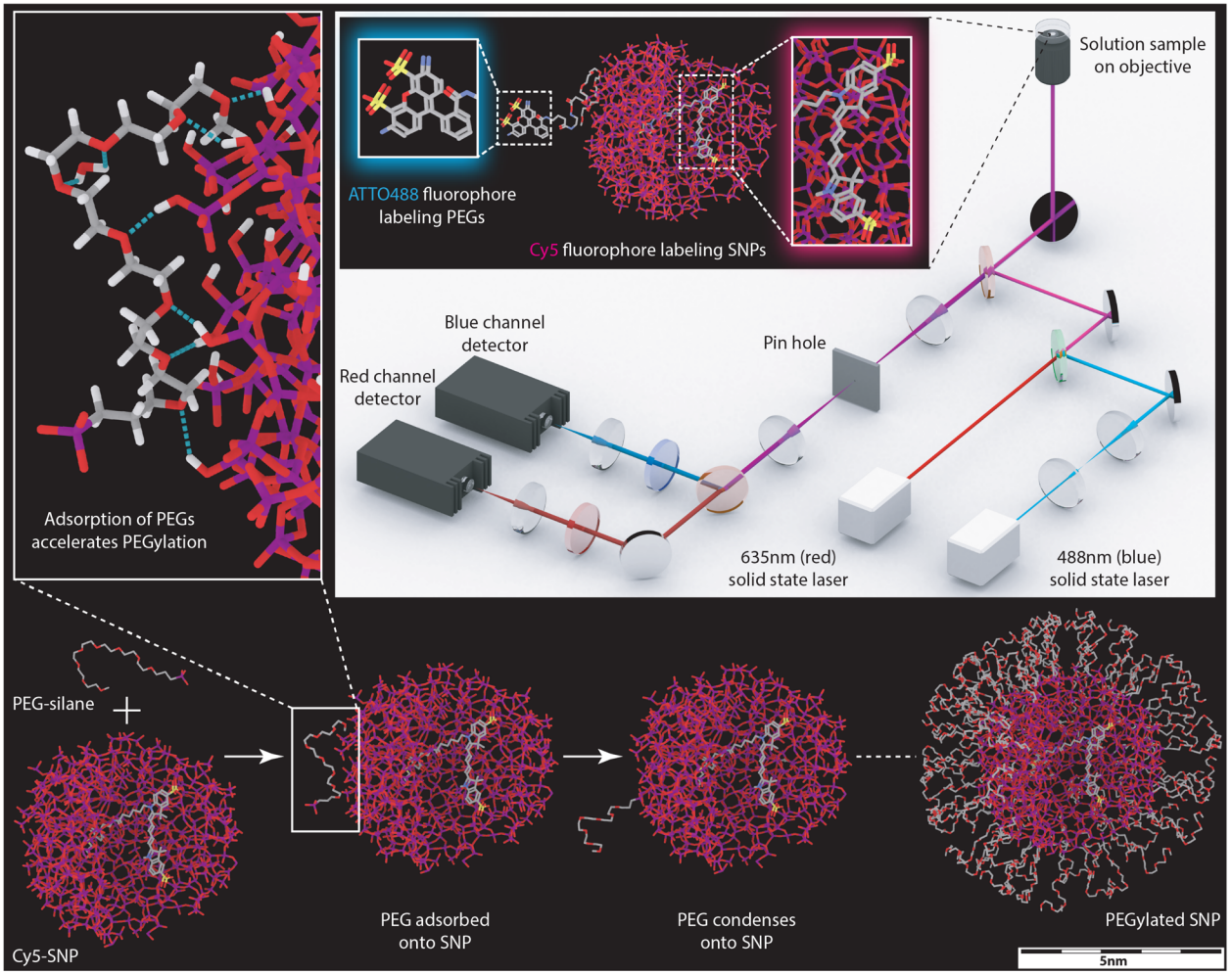

Figure 1. Illustration of SNP PEGylation mechanism as characterized by FCS and FCCS. The SNP PEGylation process (bottom) was monitored by FCS and FCCS (top right). In order to endow SNPs and PEGs with distinct fluorescence, they were labeled with Cy5 and ATTO488 fluorophores, respectively. Upon the addition of PEG-silane into SNP solution, a fast noncovalent association of PEGs and silica preceded the condensation of PEG-silane on SNP surface. The specific affinity between PEGs and silica accelerated the reaction kinetics thereby playing a key role in successful PEGylation. In the molecular renderings, silicon, oxygen, carbon, hydrogen (only shown in inset on upper left, together with hydrogen bonds in light blue), nitrogen, and sulfur atoms are color coded by purple, red, gray, white, blue, and yellow, respectively.

mobility.[32,33] Its dual-channel variant, fluorescence cross correlation spectroscopy, FCCS, simultaneously monitors the diffusion of two species with distinct fluorescence, and thus further provides information on their binding and colocalization (Figure 1).[34] FCS and FCCS have been widely applied in the field of biology to study, e.g., enzymatic reactions and protein interactions.[35,36] Their application in material science remains limited,[37,38] however, and is often confined to polymers.[39,40] Especially, the use of FCCS to analyze the processes of nanomaterial fabrication has rarely been reported. Here, after varying PEGylation reaction conditions to optimize for particle stability, we labeled SNPs and PEGs with Cy5 and ATTO488 fluorophores, respectively, and introduced FCS and FCCS to interrogate details of the PEGylation pathway (Figure 1). We found fast reaction kinetics during successful PEGylation unexpected for conventional silanol hydrolysis and condensation which prevented NP aggregation in the transition from electrostatic to steric stabilization. Effects were attributed to an instant noncovalent association of PEGs and SNP surfaces, observed even at nanomolar concentrations and accelerating covalent attachment (Figure 1). Further studies on various reaction conditions enabled the elucidation of reaction design criteria for successful PEGylation, as well as NP surface modification with functional ligands. Results highlighted that NP surface modification reactions may involve multiple processes driven by different interactions, whose understanding is critical for optimal outcomes.

EXPERIMENTAL SECTION

Chemicals and Reagents. All chemicals were used as received without further purification. Dimethyl sulfoxide (DMSO), ethanol, (3-aminopropyl)triethoxysilane (amine-silane), (3-mercaptopropyl) trimethoxysilane (thiol-silane), tetramethyl orthosilicate (TMOS), ammonium hydroxide, and polyethylene glycol (PEG 400, molecular weight 400 g/mol) were purchased from Sigma-Aldrich. 2-[Methoxy-(polyethyleneoxy)propyl] trimethoxysilane (PEG-silane, molar mass around 500 g/mol) was purchased from Gelest. Maleimido functionalized Cy5 fluorophore was purchased from GE Healthcare. Amine functionalized ATTO488 fluorophore was purchased from ATTO-Tech. NHS ester functionalized PEGs, as well as heterobifunctional PEGs functionalized with both NHS ester and maleimido, were purchased from Quanta BioDesign. c(RGDyC) peptide was purchased from Peptide International. DI water was generated using a Millipore Milli-Q system.

DOI: 10.1021/acs.chemmater.6b00030
Chem. Mater. 2016, 28, 1537−1545

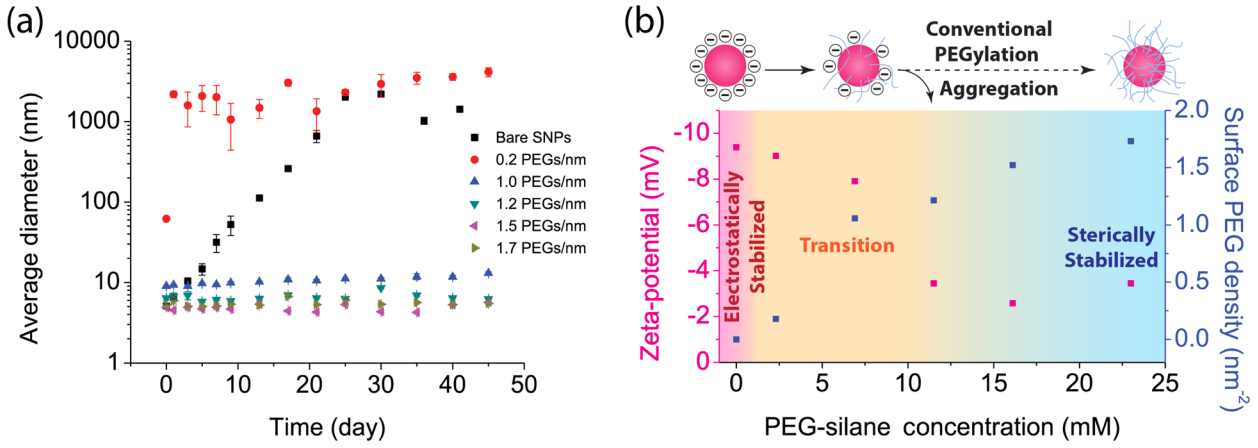

Figure 2. Long-term stability test and SNP stability transition. (a) Stability test of SNPs with varying surface PEG density in PBS buffer solution (see similar plot with linear scale in Figure S3). (b) Comparison of average zeta-potential and surface PEG density of SNPs in water (no buffer) synthesized at varying PEG-silane concentration. A gradual background color change indicates SNP stability. While the bare SNPs are electrostatically stabilized via negative surface charges (red regime), the fully PEGylated SNPs are sterically stabilized (blue regime). SNPs with surface PEG density in-between are unstable because electrostatic stabilization is greatly diminished while steric stabilization is not yet sufficient (yellow regime in part b).

Conjugation of Cy5-silane. Maleimido functionalized Cy5 was mixed with thiol-silane in DMSO at molar ratio 1:25 and concentrations of about 1 mM. The mixtures were left under nitrogen overnight to label Cy5 fluorophore with silane through thiol−ene reaction.

Conjugation of ATTO488-PEG. NHS ester functionalized PEGs were mixed with amine functionalized ATTO488 fluorophore in DMSO at molar ratio 1:1.1 and concentrations of about 10 mM. The mixtures were left under nitrogen overnight to label PEGs with ATTO488 fluorophores through amide bond formation.

Conjugation of c(RGDyC)-PEG-silane. Heterobifunctional PEGs functionalized with NHS ester and maleimido groups (NHS-PEG-mal) were first mixed with amino-silane in DMSO at molar ratio 1:1.1 and concentrations of about 10 mM. The mixtures were left under nitrogen for 2 days to label NHS-PEG-mal with silane through amide bond formation. Afterward, c(RGDyC) peptide was added into the mixture at c(RGDyC):PEG molar ratio 0.9:1. The mixtures were left under nitrogen for another day to further label mal-PEG-silane with c(RGDyC) through thiol−ene reaction.

Synthesis of Ultrasmall Silica Nanoparticles. For the synthesis of 4−5 nm silica nanoparticles, 0.02 mmol ammonium hydroxide was added into 10 mL of DI water as base catalyst.[10] A 0.43 mmol portion of TMOS was added into the solution under vigorous stirring. The stirring continued for 24 h at room temperature. If applicable, silane conjugated Cy5 fluorophore, which was obtained through mixing maleimido functionalized Cy5 and MTPMS in DMSO at molar ratio 1:25, was added together with TMOS for fluorescent SNP synthesis. Afterward, specific amounts (see main text) of PEG-silane were added, and the solution was kept stirring for another 24 h. If applicable, c(RGDyC) functionalized PEG-silane was added right before the addition of PEG-silane for the synthesis of cancer-targeting PEGylated SNPs. Following that, the temperature was increased to 80 °C, and the stirring was stopped. The reaction was left at 80 °C for 24 h. The solution was finally cooled to room temperature and transferred into a dialysis membrane tube (Pierce, molecular weight cutoff, MWCO 10 000) for dialysis. The dialysis tube was then immersed into 2000 mL of DI water, and the water was changed twice per day for 3 days to clean the PEGylated SNPs. The particles were finally filtered through a 200 nm syringe filter (Fisher) and stored at room temperature for further characterization. The molar ratio of the reactants was 1 TOMS:0.5 PEG-silane:1292 H_2O. For the synthesis of particles with varying PEG surface density, the PEG-silane concentration used in the reaction was varied from 0 to 23.0 mM.

Zeta Potential Measurements. Zeta potential of the synthesized PEGylated SNPs was measured with a Malvern Zetasizer Nano-SZ operated at 20 °C. Samples were first concentrated using spinfilters (GE Healthcare, 30k MWCO) by up to 10 times for the desired signal-to-noise ratio. Details of the zeta potential measurement optimization can be found in the Supporting Information. Each sample was measured five times, and the results were averaged.

DLS Size Measurements. Hydrodynamic particle sizes and size distributions were measured by DLS using a Malvern Zetasizer Nano-SZ system operated at 20 °C. Each DLS sample was measured five times, and the results were averaged.

TEM Measurements. TEM images were taken on a FEI Tecnai T12 Spirit microscope operated at an acceleration voltage of 120 kV. The TEM samples were prepared by dropping one droplet of the PEGylated SNP solution onto a TEM grid (EMS, carbon film on copper grids) and evaporation of solvent.

TGA Measurements. TGA was conducted using a TA Instruments Q500 thermogravimetric analyzer. Before being subjected to TGA, the synthesized PEGylated SNPs were first dried out from the aqueous solution using a FreeZone freeze-dryer. During TGA measurements, the temperature was first increased to 100 °C with a ramp rate of 10 °C/min, and kept isothermal at 100 °C for 20 min to remove the remaining water. The temperature was then increased up to 600 °C with a ramp rate of 10 °C/min and kept isothermal at 600 °C for 60 min before the sample was cooled down to room temperature.

FCS and FCCS Measurements. FCS and FCCS measurements on the various Cy5-C′ dot and ATTO488-PEG samples were conducted using a home-built FCS/FCCS setup. A 635 nm solid-state laser was used as the excitation source for the red channel, and a 488 nm solid-state laser was used as the excitation source for the blue channel. FCS and FCCS measurements usually require sample concentrations in the nanomolar range.[35] Therefore, in FCS measurements the concentration of Cy5 fluorophores added into the synthesis mixture was decreased to reduce the concentration of Cy5-labeled SNPs to nanomolar. Small amounts of the reaction solution were then aliquoted about every 1−2 min during the synthesis and directly subjected to FCS measurements without further dilution to monitor SNP growth. In FCCS measurements the concentration of added Cy5 fluorophores remained unchanged as compared to the procedures detailed in previous publications.[10] Instead, the synthesis solution was diluted in order to achieve the appropriate Cy5-C′ dot concentration.

Conductivity Measurements. Conductivity measurements were carried out using an Orion Star A215 pH/conductivity Benchtop multiparameter meter. About 24 h after TMOS addition, the conductivity probe was inserted into the reaction solution for

DOI: 10.1021/acs.chemmater.6b00030
Chem. Mater. 2016, 28, 1537−1545

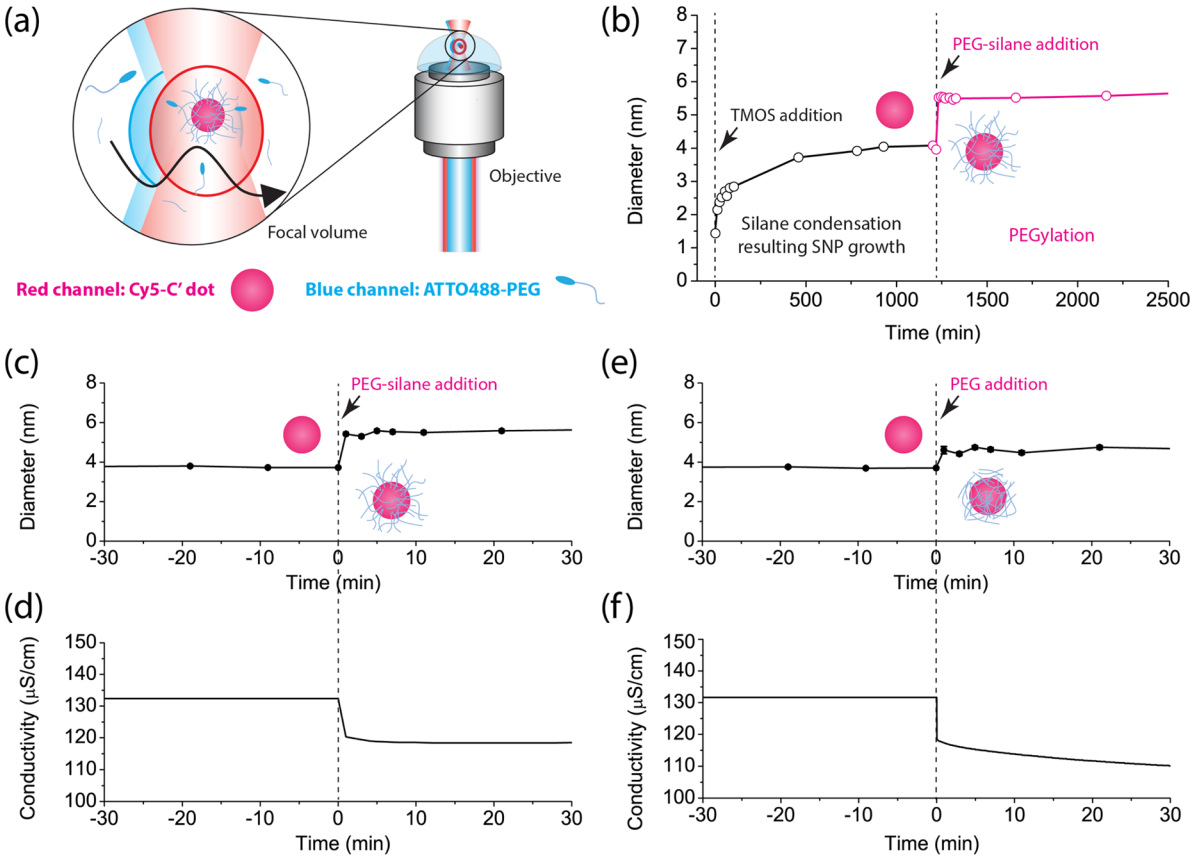

Figure 3. PEGylation process as monitored by FCS and conductivity measurements. (a) Illustration of the focal volume of FCS/FCCS setup. As fluorescence-labeled species diffuse through the focal volume, signal fluctuations are detected, and information on sample mobility and colocalization is extracted from the correlations of these signal fluctuations. (b) Change of SNP size during formation (black curve) and PEGylation (red curve) steps. (c and d) Evolution of particle size (c) and solution conductivity (d) as PEG-silane is added. (e and f) Evolution of particle size (e) and solution conductivity (f) as nonfunctionalized PEG is added.

recording the solution conductivity. After that, PEG-silane or nonfunctionalized PEG was added. To monitor the PEGylation reaction, the solution conductivity was recorded up until the high temperature treatment step.

Estimation of PEG-silane and c(RGDyC)-PEG-silane Reaction Conversion Percentage. The conversion percentage of PEG-silane with or without c(RGDyC) functionalization was estimated by taking the ratio of PEG-silane present in the final purified SNPs to the amount of PEG-silane added into the synthesis. The amount of PEG-silane (without cancer-targeting peptide functionalization) present in the final purified SNPs was estimated from TGA (provides mass) and FCS measurements (provides particle concentration). The amount of c(RGDyC)-PEG-silane present in the final purified SNPs was estimated by absorbance measurements.[10]

RESULTS AND DISCUSSION

A series of SNPs with varying surface PEG density were first synthesized according to a previously reported method in which PEGylation is an integral part of the synthesis strategy to obtain narrowly size distributed particles.[10] When the concentration of PEG-silane was increased from zero to 23 mM, the number of PEG chains per particle and surface PEG density gradually increased to about 70 PEGs/particle and 1.7 PEGs/nm^2, respectively (Table S1). The Flory radius of PEGs used in this study was about 1.7 nm, which was larger than the 0.8 nm PEG−PEG distance obtained from this surface PEG density (Supporting Information). This is consistent with full PEG coverage on the SNP surface with brush-like PEG structure (Figure 1).[41] Dynamic light scattering (DLS) and transmission electron microscopy (TEM) studies suggested that both the bare SNPs as well as the PEGylated SNPs with 1.7 PEGs/nm^2 exhibited narrow particle size distributions and homogeneous particle morphology (Figure S1). In contrast, SNPs with intermediate surface PEG densities showed reduced monodispersity due to insufficient surface PEG coverage (Supporting Information, Figures S1 and S2).

The SNPs were further transferred into PBS buffer solution for long-term stability tests. During the test period, small amounts of sample solution were aliquoted for hydrodynamic size measurements. The bare SNPs gradually aggregated in buffer solution over a period of 20−30 days (Figure 2a) due to the screening effect of surface charge by buffer salts.[42] Interestingly, at the surface PEG density of 0.2 PEGs/nm^2, the SNPs aggregated immediately after being transferred into buffer solution. As surface PEG density further increased to 1.0 PEGs/nm^2, aggregation was greatly suppressed, but a gradual increase of particle size was still observed suggesting a slow aggregation process (Figure S3). In contrast, SNPs with higher surface PEG density remained stable throughout the test period (Figure 2a and Figure S3). From the results a surface PEG density threshold for preventing SNP aggregation was estimated to be about 1.2 PEGs/nm^2. From the combination of DLS, TEM, and zeta potential measurements, however, 1.7 PEGs/nm^2 was identified as the ideal value to ensure well-PEGylated SNPs with uniform morphology, as well as narrowly

DOI: 10.1021/acs.chemmater.6b00030
Chem. Mater. 2016, 28, 1537−1545

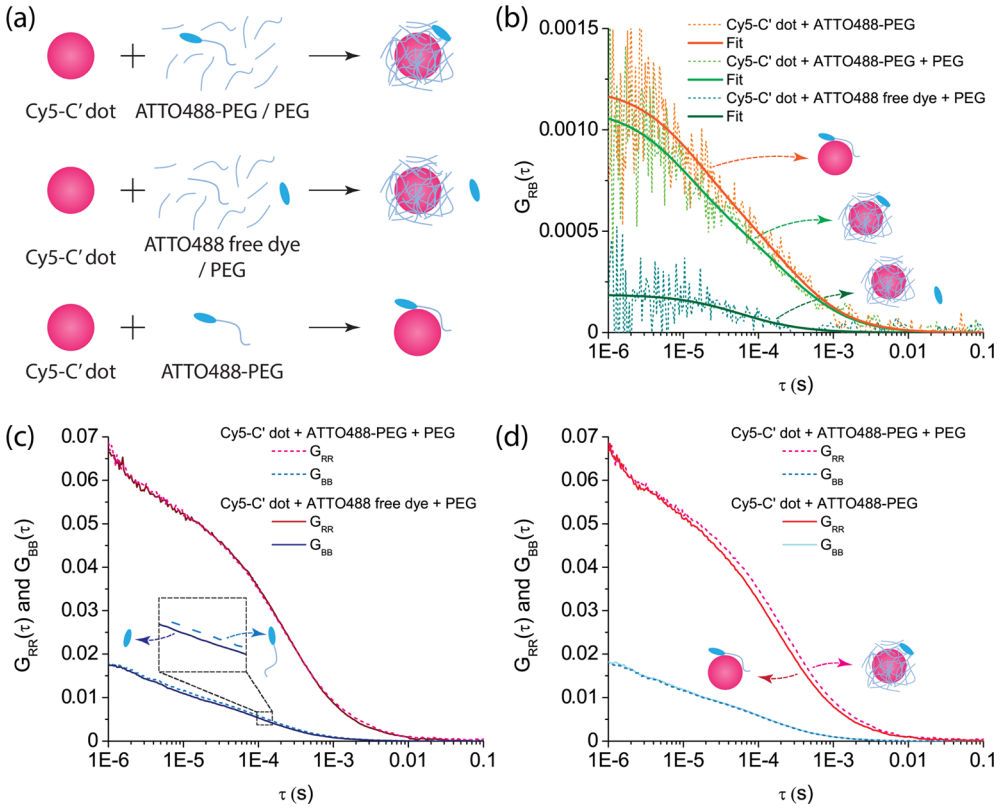

Figure 4. Association of PEGs and SNPs as characterized by FCS and FCCS. (a) Experimental designs. ATTO488-PEG/PEG (top), ATTO488 free dye/PEG (middle), and ATTO488-PEG only (bottom) were added to diluted Cy5-C′ dot solutions, respectively, and the resulting mixtures were subjected to FCS and FCCS measurements immediately after PEG addition. (b) Comparison of FCCS cross-correlation curves from all three experiments in part a. (c) Comparison of FCS red and blue channel autocorrelation curves of Cy5-C′ dot solutions to which ATTO488-PEG/PEG (top panel in a) and ATTO488 free dye/PEG (middle panel in a) were added, respectively. (d) Comparison of FCS red and blue channel autocorrelation curves of ATTO488-PEG added to Cy5-C′ dot solutions with (top panel in a) and without (bottom panel in a) extra nonfunctionalized PEGs.

distributed size distribution and zeta-potential (Figures S1 and S2).[10]

These results indicated a SNP stability transition depending on surface PEG density (Figure 2b). At neutral pH in water (no buffer) the surface of bare SNPs is covered by deprotonated silanol groups, and the resulting negative surface charge prevents particle aggregation through electrostatic repulsion (red regime in Figure 2b). On the other end of the scale the SNP surface is covalently modified with a dense layer of PEGs. Although the native surface charge is quenched, SNPs are now sterically stabilized by a neutral PEG corona (blue regime in Figure 2b). Between these two cases, when the surface PEG density gradually increases from zero to 1.2 PEGs/nm^2, the SNPs go through a transition from electrostatic to steric stabilization, as indicated, e.g., by a decrease in negative zeta-potential (yellow regime in Figure 2b). In this transition regime, SNPs lose long-range electrostatic stabilization due to a decrease in deprotonated and charged surface silanol groups, while the surface PEG density is not yet high enough to provide short-range steric stabilization. The result is particle aggregation, leading to particle precipitation or at least a broadening of the particle size distribution. It is interesting to note that the SNPs most heavily aggregated for the very low surface PEG density of ~0.2 PEGs/nm^2 (Figure 2a, and Figures S1 and S3). This suggests that electrostatic repulsion between SNPs also plays a key role in determining particle size during SNP formation, in addition to the effects of the kinetics of silane hydrolysis and condensation. Even a small decrease in SNP surface charge density may disturb the system's charge balance and lead to particle aggregation.

Because of this stability transition, fast PEGylation kinetics is highly desirable for the preparation of narrowly size dispersed PEGylated SNPs. Otherwise, SNPs may aggregate before enough PEGs condense onto the surface. In order to understand the PEGylation kinetics in more detail, we synthesized SNPs in water with Cy5 fluorophores covalently encapsulated into the core, referred to as Cy5-C′ dots, and used FCS to monitor the growth-terminating PEGylation reaction (Figure 3a and Figure S4).[10] In comparison to DLS, FCS uses fluorescence for signal processing thereby excluding any scattering noise from unreacted reagents, e.g., self-condensed PEG-silane. It is therefore highly sensitive to size changes of fluorescent SNPs during reactions. Additionally, it provides multiple parameters from a single measurement, including hydrodynamic size, concentration, and single-particle brightness,[37,43] and thus is ideally suited to reveal details of the association between particles and PEG ligands.

Figure 3b shows the change of particle size throughout the synthesis reaction over a period of about 2 days, including initial growth (black) and termination via PEGylation (red) steps (see Experimental Section for details). Bare Cy5-C′ dots with diameter around 4 nm formed during a period of about a day after injection of silica source, TMOS, and dye-silane conjugate, consistent with DLS and TEM characterization

DOI: 10.1021/acs.chemmater.6b00030
Chem. Mater. 2016, 28, 1537−1545

results (Figure S1). When PEG-silane was added to reach a concentration of 23 mM resulting in a final surface PEG density of 1.7 PEGs/nm^2, the average hydrodynamic size quickly jumped from 4 to 5.5 nm (Figure 3b and Figure S5), and then stayed fairly constant at around 5.5−6 nm for the remainder of the reaction time. The quick size increase was within the time resolution of the experiments (∼1−2 min, Figure 3c). During the same time fluorescence brightness per particle as well as particle concentration from FCS remained constant (Figure S6a,b), indicating that this immediate size increase following PEG-silane addition was not caused by particle aggregation, which in turn would lead to an increase in single particle brightness and a decrease in particle concentration. In a comparison of the size evolution of the SNP growth process via silane hydrolysis and condensation (black part) with that of the PEG-silane addition (red part) in Figure 3b, it is safe to conclude that the fast size increase is not the result of the condensation reaction between PEG-silane molecules and SNP surface silanol groups (Figure S7).[42] Instead, results point to an instant noncovalent association between PEG-silane molecules and SNPs. This interpretation is corroborated by in situ solution conductivity measurements showing a drop right after PEG-silane addition on a similar time scale suggesting the screening of SNP surface charges via PEG-silane association (Figure 3d).[44]

In order to further investigate the origin of this fast association, the same experiments were performed using PEGs without silane functionalization. Right after PEG addition, a similar particle size increase of around 1 nm and drop in conductivity were observed (Figure 3e,f and Figure S5), while particle brightness and concentration stayed unchanged (Figure S6c,d). Additional experiments further suggested that the FCS derived size increase was not the result of a viscosity increase caused by PEG addition (Figure S5c).[45]

We subsequently labeled PEGs with fluorophore ATTO488, referred to as ATTO488-PEG (Figure S8), and used FCCS to further analyze the noncovalent interaction between PEGs and silica. The red channel of the FCCS setup monitored the diffusion of Cy5-C′ dots, while the blue channel monitored the diffusion of ATTO488-PEGs (Figure 1). When PEGs are associated with SNPs, their diffusion through the focal volume is synchronized, introducing correlated signal fluctuations in both channels and thus a positive cross-correlation readout (Figure 3a), providing further colocalization information on PEGs and SNPs.[34]

The FCCS measurements require sample concentrations in the nanomolar range,[35] which is much lower than the concentrations of SNPs (around 20 μM) and PEG-silanes (around 23 mM) in the PEGylation protocol.[10] Such low reaction concentrations may change the association behavior between PEGs and SNPs. In order to circumvent this problem, we first diluted the original Cy5-C′ dot solution to about 30 nM concentration, to which a small amount of ATTO488-PEGs was added to reach about 150 nM concentration. Afterward, extra nonfunctionalized PEGs were added to raise the overall PEG concentration to 23 mM (Figure 4a, top panel). The final solution was immediately subjected to FCCS measurements. The results showed a clear cross-correlation readout (Figure 4b, light green line). The hydrodynamic size obtained from the cross-correlation was larger than 5 nm, indicating a highly specific detection of ATTO488-PEGs adsorbed onto Cy5-C′ dots (Table S2). However, the signal intensity of the cross-correlation was relatively weak as compared to the signal intensity of the autocorrelations (Figure 4b,c). This indicates the presence of large number of unattached PEGs during PEGylation, consistent with DLS results (Supporting Information, Figure S9).

To further ensure the observed association of ATTO488-PEGs and SNPs was not due to PEG functionalization with dye, the same experiments were performed with ATTO488 free dye instead of ATTO488-PEGs (Figure 4a, middle panel). The corresponding red channel autocorrelation curve overlapped with the one from the experiment using ATTO488-PEGs, both of which resulted from the PEG-adsorbing SNPs (Figure 4c, top red curves). In contrast, the blue channel autocorrelation slightly shifted to the left, confirming the faster diffusion of ATTO488 free dye as compared to that of ATTO488-PEG (Figure 4c, bottom blue curves). Finally, for this case a substantially weaker cross-correlation signal was detected (Figure 4b, dark green line), whose resulting hydrodynamic size was much smaller than what was expected from the SNP size (Table S2). This suggested that this weak cross-correlation was most likely due to leaking of fluorescence from the ATTO488 fluorophore to the red channel, rather than the specific colocalization of ATTO488 free dye and SNPs. The lack of cross-correlation signal is consistent with ATTO488 fluorophore carrying a net negative charge leading to electrostatic repulsive interactions with the negatively charged SNPs.[24] Although we observed a decreased signal-to-noise ratio due to the interchannel cross-talk and the <100% conjugation efficacy of the dyes, the obvious enhancement of cross-correlation caused by PEG conjugation of ATTO488 dye provided evidence of PEGs being adsorbed on SNP surfaces (Figure 4b).

The same experiments were also performed without the addition of extra nonfunctionalized PEGs, where both SNPs and PEGs had nanomolar concentrations (Figure 4a, bottom panel). After ATTO488-PEG addition, no increase of average SNP size was detected via the red channel autocorrelation, suggesting a substantial decrease of the amount of PEGs adsorbed onto the SNP surface due to their low concentration (Figure 4d). Despite the small amount of PEG adsorption, a strong cross-correlation signal was again detected (Figure 4b, orange line). This demonstrates that the association between PEGs and SNPs happens even at extremely low concentration, here close to the nanomolar regime. This association is due to the specific affinity between PEGs and silica, most likely caused by hydrogen bonding between the silanol groups on the SNP surface and both the ether oxygens and hydroxyl end groups of nonfunctionalized PEGs (Figure 1).[46−48]

The fast adsorption of PEGs to SNP surface quickly shortens the average distance between the silanol groups of PEG-silanes and the silanol groups on the SNP surface, thereby significantly accelerating PEG-silane condensation (Figure 1). This conclusion was supported by additional FCS experiments, showing that adsorbed PEGs without silane functionalization were released from the SNP surface upon dilution. In contrast, no release of PEG-silanes was observed, even when the SNP solution was greatly diluted immediately after PEG-silane addition (Figure S10).

Fundamental knowledge of reaction pathways allows educated design of process conditions. In order to elucidate favorable experimental conditions for PEGylation assisted by the noncovalent silica-PEG association described here, reaction solvent composition and solution pH were varied before the addition of nonfunctionalized PEGs to SNP solutions. Silica

DOI: 10.1021/acs.chemmater.6b00030
Chem. Mater. 2016, 28, 1537−1545

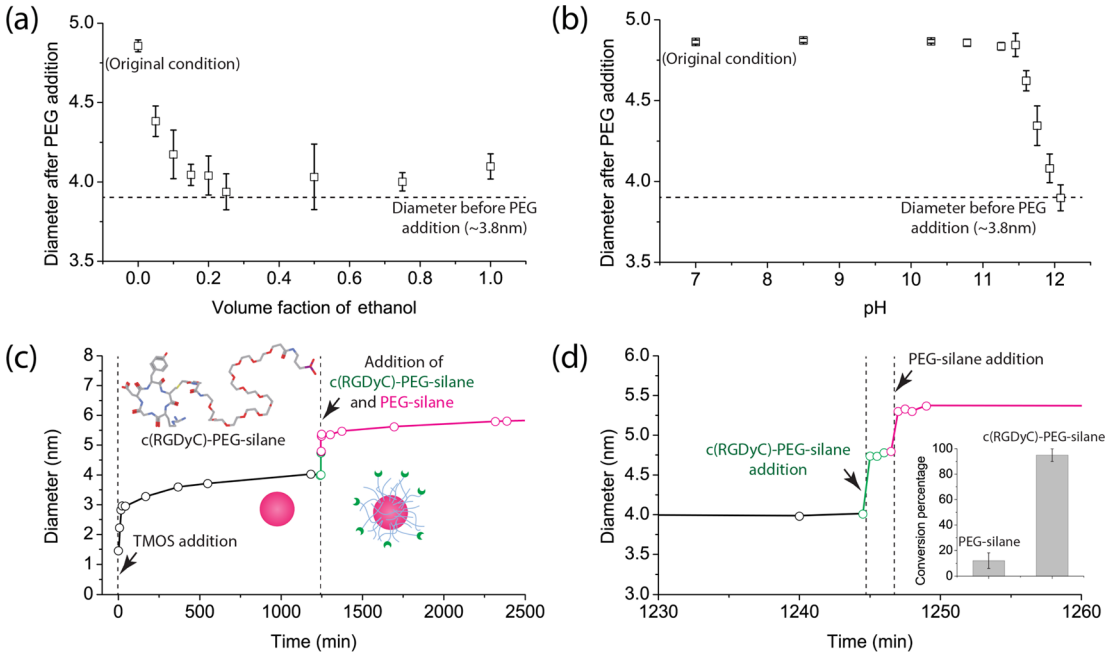

Figure 5. Association of ligands and SNPs under different conditions. (a and b) Noncovalent association between SNPs and PEGs (without silane functionalization) in aqueous solution with varying (a) volume faction of ethanol and (b) pH. The solution pH in part b was adjusted by varying the concentration of ammonium hydroxide. The dashed lines indicate SNP size before PEG addition. (c) Change of SNP size throughout a reaction in which c(RGDyC)-PEG-silane (insert) was added (green part) right before PEG-silane addition (red part) in order to surface modify the SNPs with cancer-targeting ligands. (d) Zoomed-in view of part c to the reaction period around ligand addition (color code as in part c). Comparison of the conversion percentage of PEG-silane versus c(RGDyC)-PEG-silane (insert in part d) suggests that the stronger affinity between c(RGDyC) peptides and SNPs facilitated the surface modification reaction.

PEGylation reactions are typically conducted in water, alcohol, or their mixtures. Interestingly, when the alcohol (here ethanol) fraction of the solvent mixture increased to >20%, no substantial size increase was detected anymore after PEG addition (Figure 5a). These results suggest that alcohol amounts >20% are sufficient to effectively suppress rapid PEG adsorption. In contrast, PEG adsorption was relatively insensitive to solution pH, with the association only being suppressed at relatively high values above pH 11. These data suggest that silica PEGylation reactions should be conducted at low alcohol content and under basic pH values typical for promoting silica condensation.

Our results indicate that a fast noncovalent association of PEGs and silica accelerates the formation of covalent bonds between PEG-silane and SNP surfaces, and therefore plays a key role in successful PEGylation (Figure 1). For nanomedicine applications of hybrid NPs this immediately raises the question whether similar pathways are active when reactions involve PEGs functionalized with specific targeting groups, e.g., peptides or antibodies. In order to address this question, SNPs were surface modified with PEGs conjugated to cancer-targeting peptides, c(RGDyC) (see insert in Figure 5c for molecular structure model). Cyclic RGD is known to bind to cell surface proteins (integrins), overexpressed, e.g., in melanoma, and therefore is a relevant model peptide to investigate these effects with.[27] To that end peptide functionalized and nonfunctionalized PEG-silanes were subsequently added to the same SNP solution. Upon the addition of c(RGDyC)-PEG-silane a similar instant increase of particle size as for pure PEGs was observed suggesting the immediate surface attachment of cancer-targeting groups to the SNP surface (Figure 5c). Nonfunctionalized PEG-silane added to cover the remaining SNP surface led to a second stepwise particle size increase suggesting successful PEGylation (see zoomed-in version of Figure 5c,d). The PEG−PEG distance of the c(RGDyC) functionalized particles was estimated to be about 0.8 nm and remained essentially unchanged as compared to the particles without c(RGDyC) functionalization (Supporting Information, Figure S11). It was well below the Flory radius, i.e., about 1.7 nm, indicating that the PEG chains acquired brush-like conformations on the particle surface and efficient PEGylation reaction was not affected by this additional step.

It is important to note that further analysis indicated that the conversion percentage of c(RGDyC)-PEG-silane was much higher than that of PEG-silane and began approaching 100% (insert in Figure 5d). This demonstrated an increased affinity to the silica surface of the peptide functionalized over the pure PEG-silane consistent with experience that peptides adsorb on silica surfaces.[49,50] The enhanced affinity facilitates surface modification reactions of SNPs with PEG bound peptides and may therefore substantially reduce manufacturing costs of multifunctional pharmaceutical NPs by providing high reaction yields.

CONCLUSIONS

The mechanistic details of NP PEGylation processes elucidated in this paper suggest that noncovalent association between ligand molecules, e.g., PEGs and PEG-peptide conjugates, and NP surfaces can be used to facilitate NP surface modification reactions through accelerating covalent attachment. This two-step reaction process, i.e., first adsorption and then covalent attachment, shares similarities with many biology processes. For example, in protein translation tRNA-associated amino acids

DOI: 10.1021/acs.chemmater.6b00030
Chem. Mater. 2016, 28, 1537−1545

are brought together first through specific hydrogen bond-induced interactions between ribosome and mRNA before covalent bond formation via dehydration. We expect these findings to build a foundation providing rational process design criteria not only for successful PEGylation, but also for NP surface modification with functional ligands, important in fields ranging from biosensing and bioimaging to nanomedicine. Finally, the affinity between PEGs and silica may add to the existing family of noncovalent interactions for the fabrication of novel self-assembled nanomaterials.

■ ASSOCIATED CONTENT

Supporting Information

The Supporting Information is available free of charge on the ACS Publications website at DOI: 10.1021/acs.chemmater.6b00030.

Estimation of surface PEG density, characterizations of SNPs with varying surface PEG density, optimization of Zeta potential measurements, long-term stability tests, details of FCS/FCCS setup, SNP size change upon the addition of PEG-silane and PEGs, changes of SNP concentration and brightness during PEGylation, comparison of kinetics of silane condensation and SNP PEGylation, conjugation of ATTO488 to PEGs, analysis of FCCS results, adsorption of PEGs accelerating their condensation onto SNP surfaces, and surface PEG density of c(RGDyC) functionalized PEGylated C′ dots (PDF)

■ AUTHOR INFORMATION

Corresponding Author

*E-mail: ubw1@cornell.edu.

Author Contributions

K.M. and U.W. designed the project. K.M., D.Z., and Y.C. synthesized the materials. K.M. conducted TEM, FCS, and FCCS measurements. K.M. and D.Z. conducted TGA, DLS, and zeta-potential characterizations. D.Z. conducted long-term stability tests. K.M. and Y.C. performed conductivity measurements. K.M., D.Z., Y.C., and U.W. wrote the paper. All authors read and commented on the manuscript.

Funding

National Institutes of Health, Award Number 5R01 CA161280-03; National Cancer Institute of the National Institutes of Health, Award Number U54CA199081.

Notes

The authors declare no competing financial interest.

■ ACKNOWLEDGMENTS

The authors gratefully acknowledge National Institutes of Health for the financial support under Award Number 5R01 CA161280-03. Research reported in this publication was further supported by the National Cancer Institute of the National Institutes of Health under Award Number U54CA199081. This work made use of the Cornell Center for Materials Research shared facilities supported through the NSF MRSEC program (DMR-1120296), and the Nanobiotechnology Center shared research facilities at Cornell.

■ ABBREVIATIONS

SNP, silica nanoparticle; FCS, fluorescence autocorrelation spectroscopy; FCCS, fluorescence cross-correlation spectroscopy; PEG, polyethylene glycol

■ REFERENCES

(1) *Nanomedicine Market (Neurology, Cardiovascular, Anti-Inflammatory, Anti-Infective, and Oncology Applications)—Global Industry Analysis, Size, Share, Growth, Trends and Forecast, 2013−2019*; Transparency Market Research, 2014.

(2) Chauhan, V. P.; Jain, R. K. Strategies for Advancing Cancer Nanomedicine. *Nat. Mater.* **2013**, *12*, 958−962.

(3) Torchilin, V. P. Multifunctional, Stimuli-Sensitive Nanoparticulate Systems for Drug Delivery. *Nat. Rev. Drug Discovery* **2014**, *13*, 813−827.

(4) Veiseh, O.; Tang, B. C.; Whitehead, K. A.; Anderson, D. G.; Langer, R. Managing Diabetes with Nanomedicine: Challenges and Opportunities. *Nat. Rev. Drug Discovery* **2014**, *14*, 45−57.

(5) Kotagiri, N.; Sudlow, G. P.; Akers, W. J.; Achilefu, S. Breaking the Depth Dependency of Phototherapy with Cerenkov Radiation and Low-Radiance-Responsive Nanophotosensitizers. *Nat. Nanotechnol.* **2015**, *10*, 370−379.

(6) Cho, K.; Wang, X.; Nie, S.; Chen, Z.; Shin, D. M. Therapeutic Nanoparticles for Drug Delivery in Cancer. *Clin. Cancer Res.* **2008**, *14*, 1310−1316.

(7) Harris, J. M.; Chess, R. B. Effect of Pegylation on Pharmaceuticals. *Nat. Rev. Drug Discovery* **2003**, *2*, 214−221.

(8) Petros, R. A.; Desimone, J. M. Strategies in the Design of Nanoparticles for Therapeutic Applications. *Nat. Rev. Drug Discovery* **2010**, *9*, 615−627.

(9) Guerrero-Martínez, A.; Pérez-Juste, J.; Liz-Marzán, L. M. Silica-Coated Nanomaterials: Recent Progress on Silica Coating of Nanoparticles and Related Nanomaterials. *Adv. Mater.* **2010**, *22*, 1182−1195.

(10) Ma, K.; Mendoza, C.; Hanson, M.; Werner-Zwanziger, U.; Zwanziger, J.; Wiesner, U. Control of Ultrasmall Sub-10 nm Ligand-Functionalized Fluorescent Core−Shell Silica Nanoparticle Growth in Water. *Chem. Mater.* **2015**, *27*, 4119−4133.

(11) Lin, Y.-S.; Abadeer, N.; Hurley, K. R.; Haynes, C. L. Ultrastable, Redispersible, Small, and Highly Organomodified Mesoporous Silica Nanotherapeutics. *J. Am. Chem. Soc.* **2011**, *133*, 20444−20457.

(12) Ma, K.; Sai, H.; Wiesner, U. Ultrasmall Sub-10 nm Near-Infrared Fluorescent Mesoporous Silica Nanoparticles. *J. Am. Chem. Soc.* **2012**, *134*, 13180−13183.

(13) Koole, R.; van Schooneveld, M. M.; Hilhorst, J.; Castermans, K.; Cormode, D. P.; Strijkers, G. J.; De Mello Donega, C.; Vanmaekelbergh, D.; Griffioen, A. W.; Nicolay, K.; Fayad, Z. A.; Meijerink, A.; Mulder, W. J. M. Paramagnetic Lipid-Coated Silica Nanoparticles with a Fluorescent Quantum Dot Core: A New Contrast Agent Platform for Multimodality Imaging. *Bioconjugate Chem.* **2008**, *19*, 2471−2479.

(14) van Schooneveld, M. M.; Cormode, D. P.; Koole, R.; van Wijngaarden, J. T.; Calcagno, C.; Skajaa, T.; Hilhorst, J.; t'Hart, D. C.; Fayad, Z. A.; Mulder, W. J. M.; Meijerink, A. A Fluorescent, Paramagnetic and PEGylated Gold/Silica Nanoparticle for MRI, CT and Fluorescence Imaging. *Contrast Media Mol. Imaging* **2010**, *5*, 231−236.

(15) Sun, Y.; Sai, H.; von Stein, F.; Riccio, M.; Wiesner, U. Water-Based Synthesis of Ultrasmall PEGylated Gold−Silica Core−Shell Nanoparticles with Long-Term Stability. *Chem. Mater.* **2014**, *26*, 5201−5207.

(16) Yoon, T.-J.; Yu, K. N.; Kim, E.; Kim, J. S.; Kim, B. G.; Yun, S.-H.; Sohn, B.-H.; Cho, M.-H.; Lee, J.-K.; Park, S. B. Specific Targeting, Cell Sorting, and Bioimaging with Smart Magnetic Silica Core-Shell Nanomaterials. *Small* **2006**, *2*, 209−215.

(17) Wang, Y.; Wang, K.; Zhao, J.; Liu, X.; Bu, J.; Yan, X.; Huang, R. Multifunctional Mesoporous Silica-Coated Graphene Nanosheet Used

DOI: 10.1021/acs.chemmater.6b00030
Chem. Mater. 2016, 28, 1537−1545

for Chemo-Photothermal Synergistic Targeted Therapy of Glioma. *J. Am. Chem. Soc.* **2013**, *135*, 4799−4804.
(18) Liu, J.; Wang, C.; Wang, X.; Wang, X.; Cheng, L.; Li, Y.; Liu, Z. Mesoporous Silica Coated Single-Walled Carbon Nanotubes as a Multifunctional Light-Responsive Platform for Cancer Combination Therapy. *Adv. Funct. Mater.* **2015**, *25*, 384−392.
(19) Roberts, M.; Bentley, M.; Harris, J. Chemistry for Peptide and Protein PEGylation. *Adv. Drug Delivery Rev.* **2002**, *54*, 459−476.
(20) Xia, X.-R.; Monteiro-Riviere, N. A.; Riviere, J. E. An Index for Characterization of Nanomaterials in Biological Systems. *Nat. Nanotechnol.* **2010**, *5*, 671−675.
(21) Kreyling, W. G.; et al. In Vivo Integrity of Polymer-Coated Gold Nanoparticles. *Nat. Nanotechnol.* **2015**, *10*, 619−623.
(22) Jokerst, J. V.; Lobovkina, T.; Zare, R. N.; Gambhir, S. S. Nanoparticle PEGylation for Imaging and Therapy. *Nanomedicine* **2011**, *6*, 715−728.
(23) Ow, H.; Larson, D. R.; Srivastava, M.; Baird, B. A.; Webb, W. W.; Wiesner, U. Bright and Stable Core−Shell Fluorescent Silica Nanoparticles. *Nano Lett.* **2005**, *5*, 113−117.
(24) Herz, E.; Ow, H.; Bonner, D.; Burns, A.; Wiesner, U. Dye Structure−Optical Property Correlations in Near-Infrared Fluorescent Core-Shell Silica Nanoparticles. *J. Mater. Chem.* **2009**, *19*, 6341−6341.
(25) Kim, B. H.; Hackett, M. J.; Park, J.; Hyeon, T. Synthesis, Characterization, and Application of Ultrasmall Nanoparticles. *Chem. Mater.* **2014**, *26*, 59−71.
(26) De Gennes, P. G. D. Polymer Solutions near an Interface. Adsorption and Depletion Layers. *Macromolecules* **1981**, *14*, 1637−1644.
(27) Phillips, E.; Penate-Medina, O.; Zanzonico, P. B.; Carvajal, R. D.; Mohan, P.; Ye, Y.; Humm, J.; Gonen, M.; Kalaigian, H.; Schoder, H.; Strauss, H. W.; Larson, S. M.; Wiesner, U.; Bradbury, M. S. Clinical Translation of an Ultrasmall Inorganic Optical-PET Imaging Nanoparticle Probe. *Sci. Transl. Med.* **2014**, *6*, 260ra149.
(28) Brown, W. *Dynamic Light Scattering: the Method and Some Applications*; Oxford University Press: Oxford, U.K., 1993.
(29) Butterworth, M.; Illum, L.; Davis, S. Preparation of Ultrafine Silica- and PEG-Coated Magnetite Particles. *Colloids Surf., A* **2001**, *179*, 93−102.
(30) Garcia-Fuentes, M.; Torres, D.; Martín-Pastor, M.; Alonso, M. J. Application of NMR Spectroscopy to the Characterization of PEG-Stabilized Lipid Nanoparticles. *Langmuir* **2004**, *20*, 8839−8845.
(31) Levin, C. S.; Bishnoi, S. W.; Grady, N. K.; Halas, N. J. Determining The Conformation of Thiolated Poly(Ethylene Glycol) on Au Nanoshells by Surface-Enhanced Raman Scattering Spectroscopic Assay. *Anal. Chem.* **2006**, *78*, 3277−3281.
(32) Schwille, P. Fluorescence Correlation Spectroscopy and Its Potential for Intracellular Applications. *Cell Biochem. Biophys.* **2001**, *34*, 383−408.
(33) Elson, E. L. Fluorescence Correlation Spectroscopy: Past, Present, Future. *Biophys. J.* **2011**, *101*, 2855−2870.
(34) Schwille, P.; Meyer-Almes, F.; Rigler, R. Dual-Color Fluorescence Cross-Correlation Spectroscopy for Multicomponent Diffusional Analysis in Solution. *Biophys. J.* **1997**, *72*, 1878−1886.
(35) Bacia, K.; Kim, S. A.; Schwille, P. Fluorescence Cross-Correlation Spectroscopy in Living Cells. *Nat. Methods* **2006**, *3*, 83−89.
(36) Lippincott-Schwartz, J.; Snapp, E.; Kenworthy, A. Studying Protein Dynamics in Living Cells. *Nat. Rev. Mol. Cell Biol.* **2001**, *2*, 444−456.
(37) Larson, D. R.; Ow, H.; Vishwasrao, H. D.; Heikal, A. A.; Wiesner, U.; Webb, W. W. Silica Nanoparticle Architecture Determines Radiative Properties of Encapsulated Fluorophores. *Chem. Mater.* **2008**, *20*, 2677−2684.
(38) Röcker, C.; Pötzl, M.; Zhang, F.; Parak, W. J.; Nienhaus, G. U. A Quantitative Fluorescence Study of Protein Monolayer Formation on Colloidal Nanoparticles. *Nat. Nanotechnol.* **2009**, *4*, 577−580.
(39) Jaskiewicz, K.; Larsen, A.; Lieberwirth, I.; Koynov, K.; Meier, W.; Fytas, G.; Kroeger, A.; Landfester, K. Probing Bioinspired Transport of Nanoparticles into Polymersomes. *Angew. Chem.* **2012**, *124*, 4691−4695.
(40) Schaeffel, D.; Staff, R. H.; Butt, H.-J.; Landfester, K.; Crespy, D.; Koynov, K. Fluorescence Correlation Spectroscopy Directly Monitors Coalescence During Nanoparticle Preparation. *Nano Lett.* **2012**, *12*, 6012−6017.
(41) de Gennes, P. G. Conformations of Polymers Attached to an Interface. *Macromolecules* **1980**, *13*, 1069−1075.
(42) Brinker, C. J.; Scherer, G. W. *Sol-Gel Science the Physics and Chemistry of Sol-Gel Processing*; Academic Press: Boston, 1990.
(43) Lakowicz, J. R. *Principles of Fluorescence Spectroscopy*; Plenum Press: New York, 1983.
(44) Nyffenegger, R.; Quellet, C.; Ricka, J. Synthesis of Fluorescent, Monodisperse, Colloidal Silica Particles. *J. Colloid Interface Sci.* **1993**, *159*, 150−157.
(45) Kirinčič, S.; Klofutar, C. Viscosity of Aqueous Solutions of Poly(Ethylene Glycol)s at 298.15 K. *Fluid Phase Equilib.* **1999**, *155*, 311−325.
(46) Preari, M.; Spinde, K.; Lazic, J.; Brunner, E.; Demadis, K. D. Bioinspired Insights into Silicic Acid Stabilization Mechanisms: The Dominant Role of Polyethylene Glycol-Induced Hydrogen Bonding. *J. Am. Chem. Soc.* **2014**, *136*, 4236−4244.
(47) Pochylski, M.; Aliotta, F.; Blaszczak, Z.; Gapiński, J. Structuring Effects and Hydration Phenomena in Poly(Ethylene Glycol)/Water Mixtures Investigated by Brillouin Scattering. *J. Phys. Chem. B* **2006**, *110*, 20533−20539.
(48) Derkaoui, N.; Said, S.; Grohens, Y.; Olier, R.; Privat, M. Polyethylene Glycol Adsorption On Silica: From Bulk Phase Behavior to Surface Phase Diagram. *Langmuir* **2007**, *23*, 6631−6637.
(49) Puddu, V.; Perry, C. C. Peptide Adsorption on Silica Nanoparticles: Evidence of Hydrophobic Interactions. *ACS Nano* **2012**, *6*, 6356−6363.
(50) Patwardhan, S. V.; Emami, F. S.; Berry, R. J.; Jones, S. E.; Naik, R. R.; Deschaume, O.; Heinz, H.; Perry, C. C. Chemistry of Aqueous Silica Nanoparticle Surfaces and the Mechanism of Selective Peptide Adsorption. *J. Am. Chem. Soc.* **2012**, *134*, 6244−6256.

DOI: 10.1021/acs.chemmater.6b00030
Chem. Mater. 2016, 28, 1537−1545